Experimental investigation of water droplet binary collisions and description of outcomes with a symmetric Weber number

C. Rabe, J. Malet, and F. Feuillebois

Related Articles

Deformation, breakup and motion of a perfect dielectric drop in a quadrupole electric field
Phys. Fluids 24, 032105 (2012)

The physics of aerobreakup. II. Viscous liquids
Phys. Fluids 24, 022104 (2012)

Bouncing, coalescence, and separation in head-on collision of unequal-size droplets
Phys. Fluids 24, 022101 (2012)

Thermally induced secondary atomization of droplet in an acoustic field
Appl. Phys. Lett. 100, 054101 (2012)

Stability and breakup of confined threads
Phys. Fluids 24, 012102 (2012)

Additional information on Phys. Fluids

Journal Homepage: http://pof.aip.org/

Journal Information: http://pof.aip.org/about/about_the_journal

Top downloads: http://pof.aip.org/features/most_downloaded

Information for Authors: http://pof.aip.org/authors

Experimental investigation of water droplet binary collisions and description of outcomes with a symmetric Weber number

C. Rabe,[1] J. Malet,[1,a)] and F. Feuillebois[2]

[1]*DSU/SERAC/LEMAC, Institut de Radioprotection et de Sûreté Nucléaire (IRSN), BP 68, 91192 Gif-sur-Yvette Cedex, France*
[2]*CNRS-LIMSI, BP 133, Rue J. von Neumann, 91403 Orsay Cedex, France*

The outcomes of binary collisions of water droplets are investigated experimentally for the range of parameters of a spray system used during a severe nuclear reactor accident. Droplets diameters range from 220 to 450 μm with a diameter ratio between 0.5 and 1 and impact velocities between 3 and 10 m s^{-1}. Values of the Weber number based on the small droplet size are between 20 and 280. For droplets with a Weber number up to 120, results in a map of impact parameters versus Weber number show the various regimes, namely, stretching separation, coalescence and reflexive separation. For a higher Weber number, between 120 and 280, the only observed outcomes are the two separation regimes. It is shown that results obtained for unequal droplet sizes match on a single map in terms of the impact parameter and of a new "symmetric" Weber number based on the sum of kinetic energies in the frame of the center of mass and on the sum of surface energies of the two droplets. Ashgriz and Poo ["Coalescence and separation in binary collisions of liquid drops," J. Fluid Mech. **221**, 183 (1990)] models are in agreement with our results, within experimental error. However, in this map, their representative curves depend on the diameter ratio. Simple formulas independent of the diameter ratio are therefore proposed to describe the transitions between regions representing outcomes of collisions. © *2010 American Institute of Physics.* [doi:10.1063/1.3392768]

I. INTRODUCTION

Spray systems are emergency systems designed for preserving the containment integrity in case of a severe accident in a pressurized water reactor. They are composed of over 500 interacting water droplet sprays generating droplets with diameters between 100 to 1000 μm. These systems are used to prevent overpressure, to cool down the enclosure atmosphere, to remove fission products and to enhance the gas mixing in case of presence of hydrogen in the reactor containment. Their efficiency depends on the heat and mass transfers with the surrounding gas which in turn depend on the evolution of the droplet size distribution in the containment, due to droplet collisions in the gravity field. Droplet collision, which also occurs in warm rain formation, in coating processes and in motor fuel injection, is a relevant problem for fluid dynamics. Indeed, previous experimental (Refs. 1 and 2) and theoretical (Ref. 3) papers have shown that droplet collisions may significantly modify the spray characteristics (droplet sizes and velocities). However, studying droplet interactions in a whole spray or between several impinging sprays is difficult (Refs. 4 and 5). In order to simplify this problem, binary droplet collisions were considered by many authors (Refs. 6–9). For a thorough description of the process, two steps have to be considered: (1) the determination of boundaries between the different collision outcomes in relation with the gas or liquid phase properties and

(2) the determination of the number of resulting droplets, their size and velocity. Experimental investigations of binary droplet collision were conducted using two techniques: the first one consists in suspending a single droplet in a vertical wind tunnel and providing a colliding droplet by a smaller droplet injection (Ref. 10), and the second one in bringing into contact two falling drops (Ref. 11). These results lead to the classification of five different outcomes regimes: coalescence with minor deformation, bouncing, coalescence with large deformation, reflexive separation, and stretching separation. Brazier-Smith *et al.*[1] were the first authors to propose an expression that defines the boundary between the permanent coalescence and stretching separation regimes. They used a Weber number We, calculated with the small droplet diameter d_s and the dimensionless impact parameter I

$$\text{We} = \frac{\rho d_s u_r^2}{\sigma}, \quad I = \frac{2x}{d_s + d_l}, \tag{1}$$

where u_r is the relative velocity between the droplets ($u_r = \|\vec{u}_r\|$ with $\vec{u}_r = \vec{v}_s - \vec{v}_l$), ρ and σ are the density and the surface tension of the liquid and d_l is the large droplet diameter. The dimensional impact parameter x is the distance from the center of the large droplet to the relative velocity vector originating from the center of the small droplet when at contact (see Fig. 1).

Collisions of water droplets of different sizes were also considered in past studies, with diameter ranging from 300 to 1200 μm (Ref. 12) or around 1000 μm (Ref. 13). Another dimensionless parameter, the diameter ratio $\Delta = d_s / d_l$, has

a)Author to whom correspondence should be addressed. Telephone: (33)1 69 08 87 40. Fax: (33)1 69 08 36 80. Electronic mail: jeanne.malet@irsn.fr.
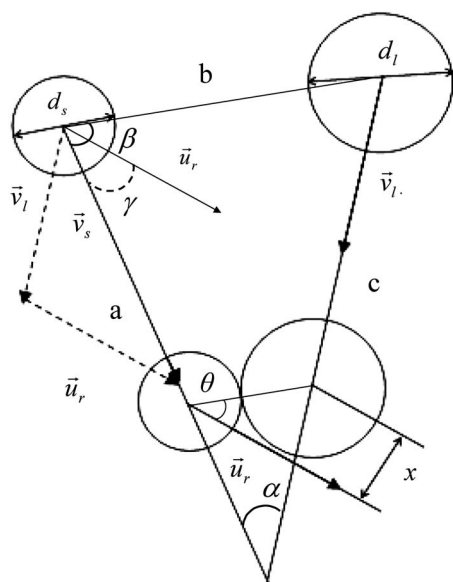
FIG. 1. Sketch of a small droplet (left) and large one (right) before collision and when at contact. α is the collision angle, (a) and (c) are the distances between the droplet centers before collision and the center of collision, and b is the distance between the droplet centers before collision.

① Pressurised deionised water supply
② Particle filter
③ Gate
④ Mass flow meter
⑤ Droplet generator
⑥ Tension Amplifier
⑦ Frequency generator
⑧ Pulse generator
⑨ Optical table
⑩ Micrometric positioning system
⑪ Xenon Lamp
⑫ CCD Camera
⑬ Picture analysis computer

FIG. 2. (Color online) Schematic description of the IRSN experimental setup for the investigation of droplets collisions.

then been introduced to describe the boundary curves. Ashgriz and Poo[6] provided some experimental results for a range of Weber number up to 120 and validated their theoretical models for the prediction of reflexive and stretching separation. The regimes appear as domains in a map in terms of (We, I). One map has to be drawn for each value of the diameter ratio. Later, spray combustion applications using hydrocarbon droplets involved the influence of liquid properties on collision outcomes (Refs. 8 and 14). The effects of the gas phase pressure and density were also analyzed experimentally, but not enough data was available to incorporate these effects in previous models. Finally, the production of satellite droplets, when collision results in break-up, is a recent subject of interest in the understanding of fundamental mechanisms that control impact outcomes (Ref. 9).

The objectives of the present work are as follows: (i) to provide an extensive database of experimental results for binary collisions of water droplets under ambient conditions; (ii) to propose a description of collision outcomes in terms of a new "symmetric" Weber number, taking into account the energies of the small and large particles in a symmetric way, which allows to collect all results for various diameter ratios on a single map; (iii) to propose new simple models describing the various boundaries in this map.

The outline of the paper is as follows. Section II presents the experimental setup and methodology. An automatic system for pictures acquisition and data treatment makes it possible to process over 200 collisions for a given value of We, thereby enhancing the accuracy of the impact parameter/Weber number maps of collisions regimes. Experimental results and a comparison with earlier works are presented in Sec. III. The new symmetric Weber number is introduced in Sec. IV together with the map for all diameter ratios in terms of this Weber number and of the impact parameter. The new
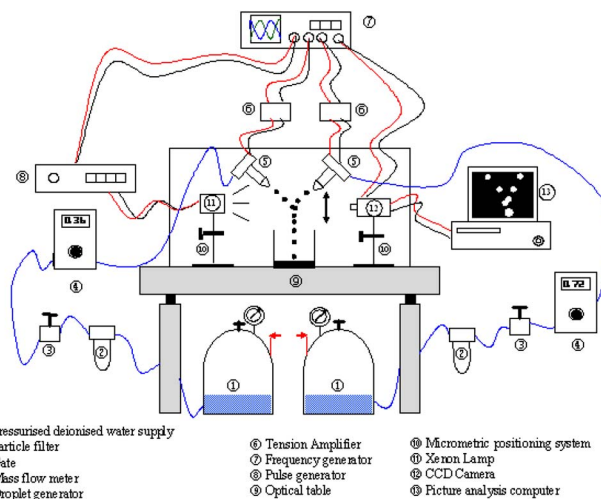
formulas for the transition curves between collision outcome domains are proposed in Sec. V. Finally, the conclusion is in Sec. VI.

II. EXPERIMENTAL SETUP AND METHODOLOGY

A. Experimental setup

A setup was built at the French Institut de Radioprotection et de Sûreté Nucléaire (IRSN), using the experience of previous experimental investigations such as Estrade.[7] It is sketched in Figs. 2 and 3.

Binary droplets collisions in a chosen vertical plane are visualized by a shadowgraphic method. Periodic drop collisions occur at the intersection of two monodispersed droplets streams. Each stream of equally spaced and similarly sized water droplets is produced by the disintegration of a liquid jet excited by an appropriate mechanical perturbation which grows in agreement with Rayleigh's theory. The use of droplets streams makes it easy to calculate the droplet velocities associated to each droplet. Moreover, the separation distance between droplets is then large enough so that the influence of
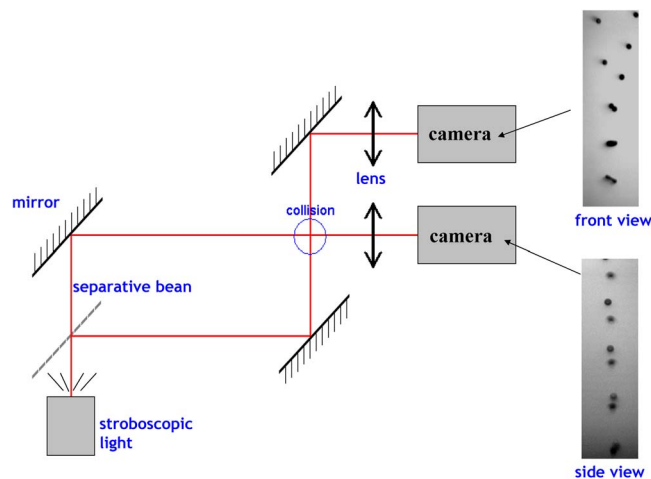

FIG. 3. (Color online) System for recording periodic droplet collisions.

the neighboring droplets, that might modify the evaporating rate as well as the drag coefficient (Ref. 15), is negligible.

The droplet generator developed at ITLR (Institute für Thermodynamik der Luft und Raumfahrt, Stuttgart), see, e.g., Frohn and Roth,[11] creates such a perturbation of the liquid jet by varying the electrical frequency excitation of a piezoelectric ceramic. The droplet diameter and velocity of the produced monodisperse spray range, respectively, from 200 to 700 μm and from 1 to 6 m/s, depending on the diameter of an exchangeable orifice (iridium plates with a hole of 90, 150, 200, and 250 μm), on the flow rate (0.2–1 kg/h) and on the excitation frequency (2000–15 000 Hz). The liquid used for the experiments was de-ionized water. It is supplied by an air pressurized water tank, through a 0.1 μm particle filter before reaching the droplet generator, as shown in Fig. 3. The liquid can thus be considered as very pure. The flow rate is controlled with two Bronkhorst© mass flowmeters (with a delivering range up to 2 kg/h) connected to the droplet generator. Since the droplet diameter depends also on the excitation frequency, this one is modulated using two Tektronix© arbitrary function generators producing a square signal up to 30 kHz. This signal with an amplitude of 10 V is amplified to 60 V with two NF© high-speed bipolar amplifiers before exciting the piezoelectric ceramic. When experimental parameters are established, collisions are recorded by two charge coupled device cameras (with square pixels of 8 μm) with appropriate enlarging optical lenses in order to observe only the area of interest. Both front and side views are recorded at the same time using a High-Speed Photo-System© stroboscopic light (with a very short flash duration of 150 ns ensuring a "frozen" droplet motion), as described in Fig. 2. The first camera delivers the pictures to be analyzed and the second one is used to align the two droplets streams in a same vertical plane. A transistor-transistor logic (TTL) signal provided by the frequency generators and the cameras is sent to the stroboscope through a synchronization device, so that the flash is switched on when the camera shutter is open. The positions and angles of the droplet streams, mirrors and cameras are adjusted by a micrometric x-y-z axis displacement system placed on an optical table in order to avoid any vibration. This system also allows to modify the collision angle and distance between the droplet streams; thereby fixing the impact parameter and the impact velocity in the range from 3 to 10 m s^{-1}. Pictures recorded in this way (typical examples are presented in Fig. 4) are analyzed with a self-made JAVA program in order to determine the Weber number and impact parameter of the recorded collision.

B. Measurement method

The measurement method consists in recording sequences of one hundred pictures of collisions for each value of the Weber number. Then, images are grouped with regard to their quality: the ones that suffer from various defects, such as a lack of light or missing droplets, are rejected and the other ones are checked with a program specially developed for that purpose using the IMAGEJ software.

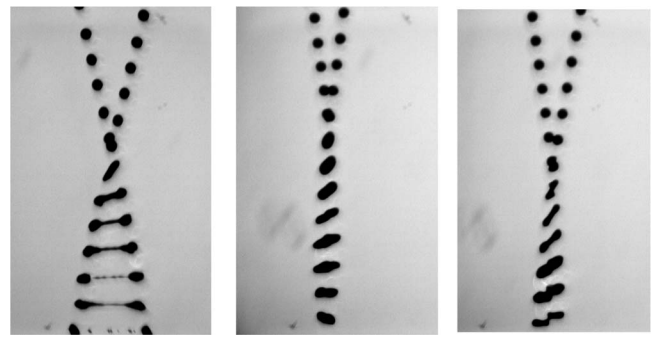A first step, which consists in calibrating the excitation

FIG. 4. Pictures of the three different binary water collision outcomes observed on the experimental setup used in this study (from left to right: stretching separation, coalescence, and reflexive separation).

frequency, the picture scale and the particles detection conditions (drops light level, size, and circularity range) in the dedicated field, is done just before running the analysis. The scale is determined with a calibrated reticule. Then, the program calculates the Weber number, We and the nondimensional impact parameter I in each picture. It first performs a binary treatment process in order to detect each fluid particle (using boundary detection conditions defined beforehand) and evaluates its size and the coordinates of its center. After sorting out to which stream the droplets belong (viz., the left one or the right one), it determines the droplets velocity, multiplying the average distance between them by the excitation frequency. The Weber number is then calculated from these data. The calculation of the impact parameter starts by an estimation of the coordinates of the intersection point of the streams. Then, the distance from the last drop of each stream to the intersection point is determined. Finally, Al-Kashi's relations [see Eq. (2) below] provide the expression of the angle β between the sides a and b of the triangle sketched in and the angle γ between the relative velocity $\vec{u}_r$ and the side a, so as to obtain the dimensionless impact parameter

$$\beta = \cos^{-1}\left(\frac{a^2+b^2-c^2}{2ab}\right), \quad \gamma = \sin^{-1}\left(\frac{\|\vec{v}_l\|}{\|\vec{u}_r\|}\sin\alpha\right),$$

$$I = \frac{2b\sin|\beta-\gamma|}{d_l+d_s},$$

(2)

where $\vec{v}_l$ is the velocity of the large droplet and α the angle between the droplet velocities.

The largest measurement error came from the number of pixels representing a droplet diameter, i.e., typically 25 pixels across a 220 μm droplet. Since one pixel could be missed or added at each end of the diameter, this gave an overestimate of 8% error. As a result, errors on We and I were estimated to be 8% and 10%, respectively.

III. EXPERIMENTAL RESULTS FOR DIFFERENT SIZE RATIOS Δ

In order to characterize the influence of the droplet size dispersion on collision outcomes for sprays used in nuclear containment, the effects of the diameter ratio Δ on transition curves between regimes was explored by performing experi-
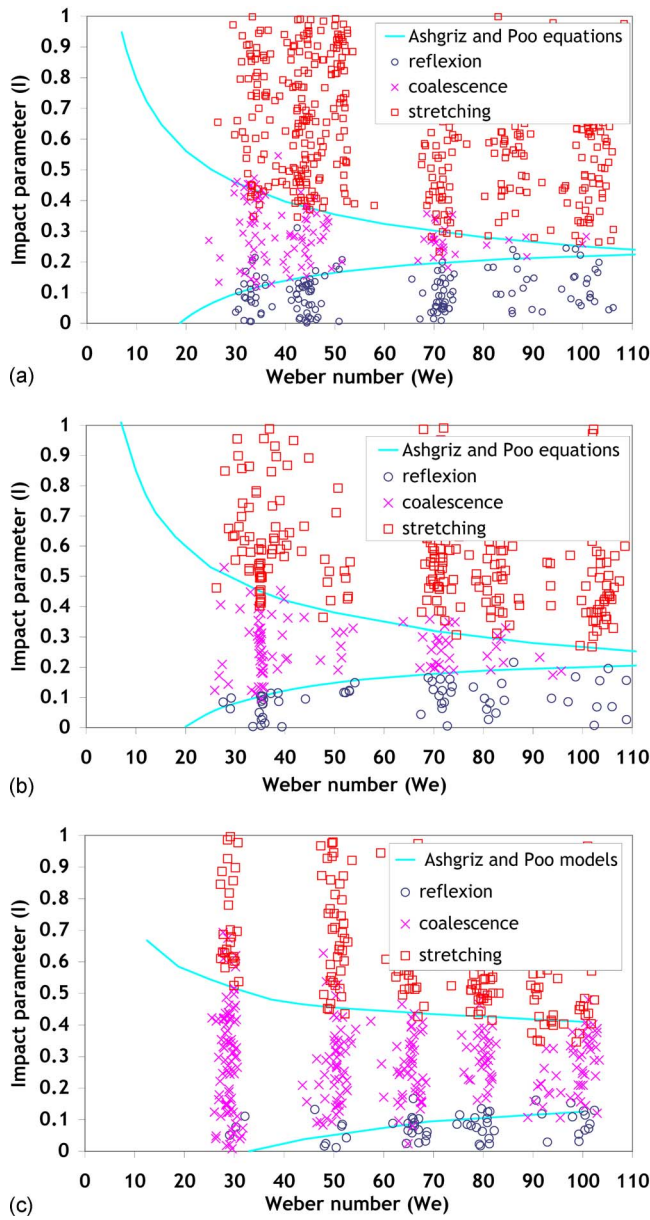
FIG. 5. (Color online) Experimental results for collision outcomes with water droplets of different diameters. Solid lines represent Ashgriz and Poo (Ref. 6) models for the boundaries between collision outcomes. (a) $d=450$ μm, $\Delta=1$, (b) $d_1=450$ μm, $d_2=330$ μm, $\Delta=0.75$, and (c) $d_1=450$ μm, $d_2=225$ μm, $\Delta=0.5$.

ments for $\Delta=0.5$ with droplets of 220 and 450 μm, and for $\Delta=0.75$ with droplets of 330 and 450 μm. Results are presented in Fig. 5.

It is observed that the boundary limits between coalescence and separation outcomes become wide apart as the diameter ratio decreases (a) $\Delta=1$, (b) $\Delta=0.75$, and (c) $\Delta=0.5$) and, as a consequence, the coalescence regime is enhanced. Indeed, when the diameter ratio decreases, the kinetic energy of the small droplet is not sufficient to overcome the surface energy of the large one; thereby reducing the possibility of occurrence of a stretching separation. Presented results are also in good agreement with Ashgriz and Poo[6] formulas, plotted as solid lines. These formulas have been used in many earlier works to describe domains in the

impact parameter/Weber number map for collision outcomes. It should be emphasized that Ashgriz and Poo's formulas were only partially verified until now, according to Orme.[16] Now, since the obtained curves depend widely on the droplet diameter ratio Δ, it appears appropriate to search for a more general map that would encompass all cases. In this goal, we revisit in Sec. IV the relevance of the Weber number, We, which is usually used for such experiments.

IV. THE SYMMETRIC WEBER NUMBER

Many papers dealing with the subject of droplet collision (Refs. 1 and 2) use the same expression of the Weber number (We) for the description of the different outcomes. This number, expressed in Eq. (1), depends on the small droplet diameter d_s and the relative velocity u_r. It looks appropriate for two equal droplets or for a droplet and a flat interface. However, for intermediate situations of unequal droplets, there is no reason to omit properties of the large droplet altogether. To avoid this restriction, Jiang et al.[8] gave another expression of a Weber number using the average of the two diameters and the relative velocity. Even so, this improvement cannot clearly identify the incoming kinetic and surface energies responsible for the collision outcome.

Since the Weber number is the ratio of a kinetic energy to a surface energy, starting from mechanical first principles dictates appropriate choices for these energies as the sum of kinetic energies of incoming droplets and the sum of their surface energies

$$We_s = \frac{\frac{1}{2}m_s\|\vec{u}_s\|^2 + \frac{1}{2}m_l\|\vec{u}_l\|^2}{\sigma\pi d_s^2 + \sigma\pi d_l^2}, \tag{3}$$

where m_s and m_l are the mass of the small and large droplet, u_s and u_l the velocities relative to the center of mass of the incoming droplets; these velocities are the only relevant ones for the collision. Using the momentum balance,

$$m_s\vec{v}_s + m_l\vec{v}_l = (m_s + m_l)\vec{v}_g, \tag{4}$$

the velocity $\vec{v}_g$ of the center of mass is obtained and the velocities relative to the center of mass are calculated as $\vec{u}_s=\vec{v}_s-\vec{v}_g$ and $\vec{u}_l=\vec{v}_l-\vec{v}_g$. Assuming that the droplets are spherical and have the same uniform density, Eq. (4) gives

$$\vec{v}_g = \frac{d_s^3\vec{v}_s + d_l^3\vec{v}_l}{d_s^3 + d_l^3}, \tag{5}$$

and the definition (3) then writes

$$We_s = \frac{\rho}{12\sigma}\frac{d_s^3\|\vec{u}_s\|^2 + d_l^3\|\vec{u}_l\|^2}{d_s^2 + d_l^2}. \tag{6}$$

Since it is symmetric in the properties of the large and small droplets, we call it the "symmetric Weber number," to distinguish it from the generally used We.

We calculated this symmetric Weber number We_s for each of the collision points presented above, using droplet parameters given by the image postprocessing. Results for the collision outcomes in terms of this number are presented in Fig. 6 for the three different diameter ratios (a) $\Delta=1$, (b) $\Delta=0.5$, and (c) $\Delta=0.75$).
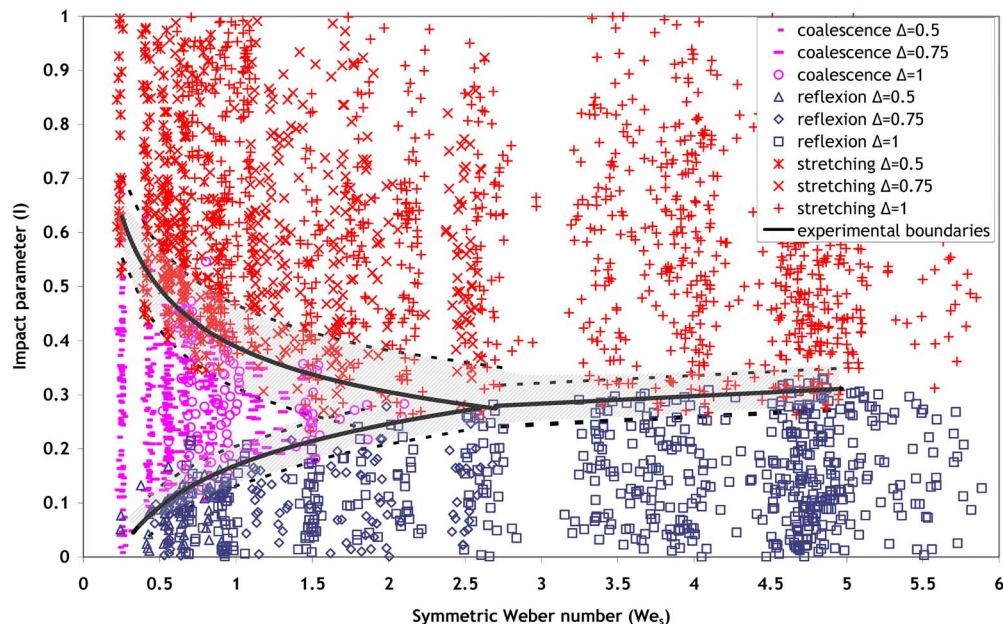
FIG. 6. (Color online) Experimental results of collision outcomes. Fitted curves delimiting the various regimes with their associated shaded domain (limited by dashed lines) representing the 99.74% confidence interval (± 3 standard deviations).

It is first noticed that values of We_s at the boundaries between coalescence and separation (either reflexion of stretching) are of order unity, corresponding thus to a better description of the competition between surface tension and inertial effects. Moreover, when using the symmetric Weber number We_s, all boundaries between domains of collision issues become independent of the diameter ratio Δ. That is, the merging of experimental results directly provides critical values of the impact parameter I_c, which define transition curves between the various outcomes. The suppression of the droplet diameter ratio as a required parameter for determining the collision issue is an important experimental result and a guidance for theoretical models.

For a more precise account of this merging of curves, it should be remarked that there is always some overlap between regimes due to experimental uncertainties. The boundaries between regimes were thus determined in a systematic way as follows. For a small interval around a given We_s, the number of collision issues belonging to each regime was counted as a function of the impact parameter I. A distribution function was defined for each collision outcome regime as the ratio of the number of points belonging to this regime to the total number of points of both regimes. The critical I_c was then defined as the impact parameter for which both distribution functions were equal to 50%. This procedure is justified since the density of experimental points is quite large and estimated to be uniformly distributed among the values of the impact parameter. This calculation was done with a VISUAL BASIC program. The resulting values for I_c were fitted with a curve. The standard deviation of the differences between the curve and the experimental I_c was calculated and found to be consistent with the error estimates of Sec. II B. The three curves obtained in this way are represented in Fig. 6 together with an associated shaded domain showing the 99.74% (± 3 standard deviations) confidence

interval. These transitions curves give an accurate representation of the experimental transitions between the various outcomes.

V. SEMIEMPIRICAL MODELING FOR TRANSITION CURVES BETWEEN COLLISION OUTCOMES IN TERMS OF THE SYMMETRIC WEBER NUMBER

A. Comparison with former models

First, it is useful to express the symmetric Weber number in terms of We that is widely used in the literature. Rewriting Eq. (6) in terms of the diameter ratio

$$We_s = \frac{\rho d_s}{12\sigma} \frac{\Delta^3 \|\vec{u}_s\|^2 + \|\vec{u}_l\|^2}{\Delta(1+\Delta^2)}, \tag{7}$$

and using (4)

$$\begin{cases} \|\vec{u}_l\| = \dfrac{\Delta^3}{1+\Delta^3}\|\vec{u}_r\|, \\[2mm] \|\vec{u}_s\| = \dfrac{1}{1+\Delta^3}\|\vec{u}_r\|, \end{cases} \tag{8}$$

we obtain

$$We_s = \frac{\rho d_s \|\vec{u}_r\|^2}{\sigma} \frac{\Delta^2}{12(1+\Delta^3)(1+\Delta^2)}$$

$$= We \frac{\Delta^2}{12(1+\Delta^3)(1+\Delta^2)}. \tag{9}$$

The new Weber number formulation is then introduced in the Ashgriz and Poo formulas (see the Appendix). For the transition between reflexive separation and coalescence, Eq. (A1) is then transformed to
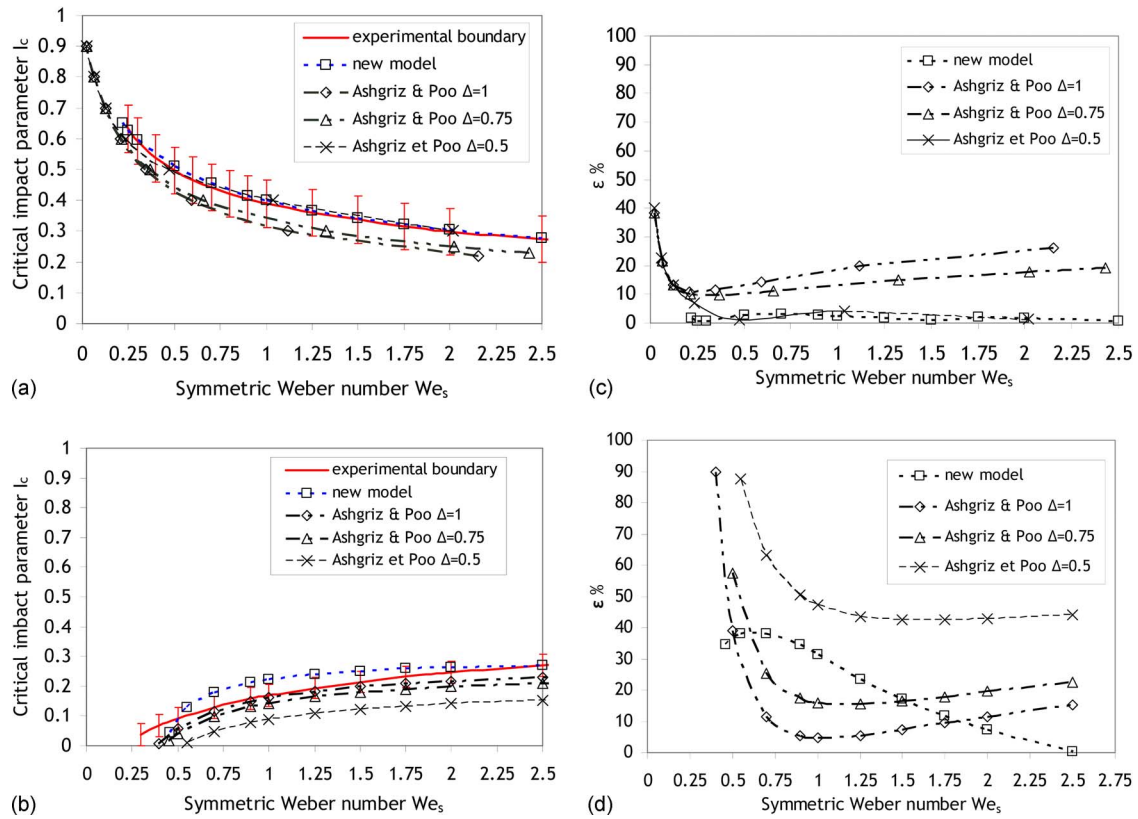
FIG. 7. (Color online) Curves for outcomes transitions: [(a) and (c)] coalescence/stretching separation and [(b) and (d)] coalescence/reflexive separation. Left: critical impact parameter, error bars represent ± 3 standard deviations. Right: relative difference on I_c between the experimental results, and both Ashgriz and Poo (Ref. 6) expressions ($\Delta = 0.5; 0.75; 1$) and the new proposed model.

$$\mathrm{We}_{sI} = \left[\frac{(7(1 + \Delta^3)^{2/3} - 4(1 + \Delta^2))\Delta^3(1 + \Delta^3)}{4(\eta_2 + \Delta^6 \eta_1)(1 + \Delta^2)} \right], \quad (10)$$

where the functions η_1, η_2 of (I, Δ) are defined in the Appendix.

In the same way, for the transition between stretching separation and coalescence, it is found from Eq. (A3) in the Appendix

$$\mathrm{We}_{sII} = \frac{(1 + \Delta^3)[3(1 + \Delta)(1 - I)(\Delta^3 \Phi_s + \Phi_l)]^{1/2}}{3(1 + \Delta^2)[(1 + \Delta^3) - (1 - I^2)(\Phi_s + \Delta^3 \Phi_l)]}, \quad (11)$$

where the functions Φ_s, Φ_l of (I, Δ) are defined in the Appendix.

Formulas (10) and (11) are compared in Fig. 7 to experiment, viz., to the fitting curves from Fig. 6 delimiting outcomes domains. Equation (11) is represented in b (and its relative error in d) and Eq. (10) in a (and its relative error in b). The formulas depend on the droplet diameter ratio Δ. It appears in Fig. 7(b) that the interval of three standard deviations is still not sufficient to include the Ashgriz and Poo expression for all Δ's. Indeed, it is remarked in Figs. 7(b) and 7(d) that the difference with our experiments is small for $\Delta = 1$ but increases for decreasing Δ. It is still small for $\Delta = 0.75$ but increases widely for $\Delta = 0.5$. This behavior may be understood when comparing the two Weber numbers. The variation of the $\mathrm{We}_s/\mathrm{We}$ ratio with the droplet diameter ratio is plotted in Fig. 8. It clearly appears that this ratio is prac-

tically constant, within experimental error between $\Delta = 1$ and $\Delta = 0.75$, but is quite lower for $\Delta = 0.5$. This shows why the classical Weber number was so successful in despite of its *ad hoc* definition: in the range of diameter ratios from 0.75 to 1, it is practically proportional to the symmetric Weber number which appears (Fig. 6) appropriate to describe various diameter ratios. This is also a reason why Ashgriz and Poo[6] models based on the classical Weber number are good approximations in this range between $\Delta = 1$ and $\Delta = 0.75$ but not so good for smaller Δ.

Considering that experimental results were merged in Fig. 6 in a map independent of Δ, it appears thus appropriate to derive simple formulas expressing the boundaries of collision outcomes in this map. Two expressions are proposed in Secs. V B and V C for the determination of the boundaries between the coalescence, stretching and reflexive separation domains.

B. Model for transition curve between reflexive separation and coalescence

According to photographs of reflexive separation obtained using the experimental device presented above, it clearly appears that for a fixed Weber number complete front collisions ($I \approx 0$) lead to a quicker droplet separation than those with a small impact parameter ($I > 0$). When the impact parameter I increases, the set of merged droplets is stretched horizontally, provoking a parasite loss of energy.
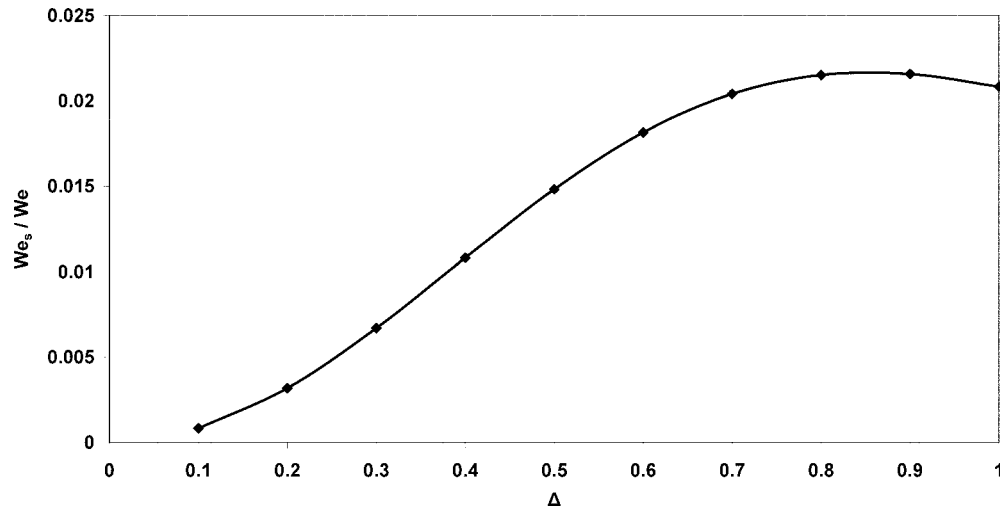
FIG. 8. Ratio of the symmetric Weber number We_s to the Weber number We.

This phenomenon is countered by surface tension forces that tend to minimize the liquid surface. Nevertheless, as a consequence of this stretching, a part of the total kinetic energy is still lost during the collision. A way to apply these observations in the modeling of the reflexion/coalescence transition curve is to consider the competition between the kinetic energy based on the drop velocities projected on the line joining their centers and the surface energy. This kinetic energy decreases when the impact parameter increases. Our assumption here is that the transition from reflexive separation to coalescence is achieved when the surface energy becomes higher than this part of the kinetic energy.

By referring to the definitions of the impact parameter I and angle θ described in

$$\sin \theta = I. \tag{12}$$

Then the droplets velocities along their line of centers are, in the frame of the center of mass (Fig. 9)

$$v_{lx}^2 = v_l^2 \cos^2 \theta = v_l^2 (1 - I^2), \tag{13}$$

$$v_{sx}^2 = v_s^2 \cos^2 \theta = v_s^2 (1 - I^2). \tag{14}$$

The total kinetic energy corresponding to these velocities, $E_{\mathrm{kin}\ x}$, may be expressed in term of the total kinetic energy E_{kin}, as

$$E_{\mathrm{kin}\ x} = E_{\mathrm{kin}}(1 - I^2). \tag{15}$$

Let the efficient kinetic energy responsible for possible reflexion, E_{eff}, be the difference between $E_{\mathrm{kin}\ x}$ and an energy dissipated by viscous effects. This dissipation is a fraction of the total kinetic energy, since it depends on liquid movements taking place into the drop formed just after the collision. The efficient kinetic energy is

$$E_{\mathrm{eff}} = E_{\mathrm{kin}\ x} - k E_{\mathrm{kin}}. \tag{16}$$

In the expression proposed here, k is assumed to be a constant for simplicity. The transition between coalescence and reflexive separation is related to values of the ratio of this efficient kinetic energy E_{eff} to the surface energy. By analogy to a Weber number, it is denoted here We_{eff}

$$We_{\mathrm{eff}} = \frac{E_{\mathrm{eff}}}{E_{\mathrm{sur}}} = \frac{E_{\mathrm{kin}}(1 - I^2) - k E_{\mathrm{kin}}}{E_{\mathrm{sur}}}. \tag{17}$$

That is, in term of the symmetric Weber number

$$We_{\mathrm{eff}} = We_s(1 - I^2 - k). \tag{18}$$

For a zero value of the impact parameter I, our experimental results indicate that the transition between the two outcomes appears for a Weber number We_{re} of around 0.45. We therefore derive the value

$$k = 1 - \frac{We_{\mathrm{eff}}}{We_{re}}. \tag{19}$$

From the previous expression, the critical impact parameter I_c for transition is

$$I_c = \sqrt{\frac{We_{\mathrm{eff}}}{We_{re}}} \sqrt{1 - \frac{We_{re}}{We_s}}. \tag{20}$$

Moreover, when the Weber number becomes large, experimental measurements give a critical impact parameter $I_c = 0.28$ for the boundary of the two regimes. We then derive from $We_{re} = 0.45$ the value $We_{\mathrm{eff}} = 0.035$ and consequently $k = 0.92$. The final expression for the transition between the reflexive separation and coalescence is then given as follows:

$$I_c = 3.59 \sqrt{1 - \frac{0.45}{We_s}}, \tag{21}$$

and presented as the "new model" in Fig. 7(b). The formula captures the essential experimental features in despite of its simplicity. The error for intermediate Weber numbers, Fig. 7(d) may originate from our rough approximation for the dissipation.

Expressing the dissipation in terms of a single constant coefficient k is possible here due to the low viscous dissipation in water. For a more viscous liquid, it is known that the boundaries between regimes depend on fluid viscosity, as shown by Gotaas et al.[17] Thus, changes are expected in the charts in terms of the new symmetric Weber number. It is clear that the k coefficient introduced here to represent vis-
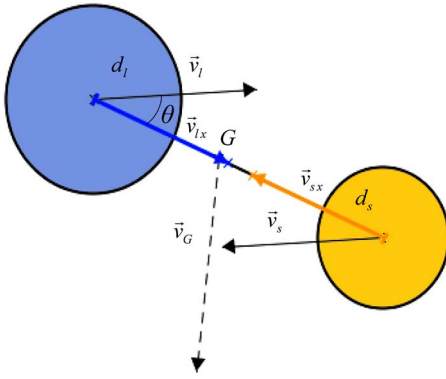
FIG. 9. (Color online) Droplets velocities projected onto the line joining their centers in the mass center reference frame.
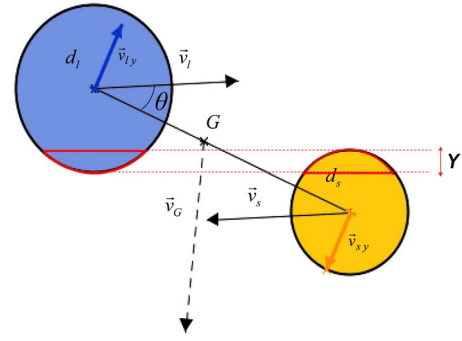

FIG. 10. (Color online) Droplet velocities are projected on the perpendicular to the line joining the center in the mass center reference frame. Y denotes the penetration length.

cous dissipation would increase for a more viscous liquid. However, the way in which it would increase is not clear and further studies are needed.

C. Model for transition curve between coalescence and stretching separation

It clearly appeared on experimental photographs that a larger impact parameter I enhances the stretching of the droplet set formed after collision. It was also observed that, for a given value of the Weber number, separation occurs earlier for a higher impact parameter. It may be thus assumed that the collision outcome depends on the competition between the kinetic energy of this stretching motion and the surface energy. That is, when this stretching kinetic energy decreases, at low impact parameter, the coalescence outcome appears. The main assumption of this model amounts to take into account only the component of droplets velocities that contribute to the stretching phenomenon in the evaluation of the kinetic energy. These components, see Fig. 10, are obtained by projecting drops velocities in the frame of the mass center on the perpendicular to the line joining the centers. Considering the θ angle and the impact parameter, these velocity components are

$$v_{ly}^2 = v_l^2 \sin^2 \theta = v_l^2 I^2, \tag{22}$$

$$v_{sy}^2 = v_s^2 \sin^2 \theta = v_s^2 I^2. \tag{23}$$

The stretching kinetic energy is then

$$E_{\text{kin }y} = E_{\text{kin}} I^2. \tag{24}$$

The surface energy which opposes kinetic effects is represented by the parts of droplets that interact during the collision. It is assumed that the surfaces of interaction S_s and S_l of the small and large droplet, respectively, depend on a penetration length Y (see Fig. 10) defined as

$$Y = (r_s + r_l)(1 - I). \tag{25}$$

They are defined as

$$S_l = 2\pi r_l Y, \tag{26}$$

$$S_s = 2\pi r_s Y. \tag{27}$$

Thus, the total interacting surface energy is given by

$$E_{\text{sur }y} = 2\pi\sigma(r_s + r_l)^2(1 - I) = E_{\text{sur}} \frac{(r_s + r_l)^2}{2(r_s^2 + r_l^2)}(1 - I), \tag{28}$$

with E_{sur} corresponding to the sum of surface energies of the initial droplets.

A "stretching Weber number" which would be of order unity at the transition between stretching separation and coalescence is then expressed by

$$\text{We}_{\text{stretch}} = \frac{E_{\text{kin }y}}{E_{\text{sur }y}} = \text{We}_s \frac{2I^2}{(1 - I)} \frac{r_s^2 + r_l^2}{(r_s + r_l)^2}. \tag{29}$$

Moreover, since $0 \leq \Delta \leq 1$, it is remarked that

$$\frac{1}{2} \leq \frac{r_s^2 + r_l^2}{(r_s + r_l)^2} = \frac{1 + \Delta^2}{(1 + \Delta)^2} \leq 1. \tag{30}$$

That is, this ratio stays of order unity. Thus, a simple approximation for the stretching Weber number is

$$\text{We}_{\text{stretch}} \approx \text{We}_s \frac{2I^2}{(1 - I)}. \tag{31}$$

Solving for I provides an expression for the critical impact parameter at the transition between stretching separation and coalescence

$$I_c = \frac{\sqrt{\text{We}_{\text{stretch}}^2 + 8\text{We}_{\text{stretch}}\text{We}_s} - \text{We}_{\text{stretch}}}{4\text{We}_s}. \tag{32}$$

From our experimental results, this expression gives a correct representation of the boundary curve between the two regimes for $\text{We}_{\text{stretch}} = 0.53$. Indeed, the comparison shown in Fig. 7(a) (see the new model) is excellent, as detailed by the error plotted in Fig. 7(c). It has to be noticed that this new model does not take into account the viscous dissipation effects that should be less important than for reflexive separation because of a minor liquid volume engaged in the stretching regime. This is probably why, without any approximation on the dissipation, this criterion is more precise than the one in Sec. V B.
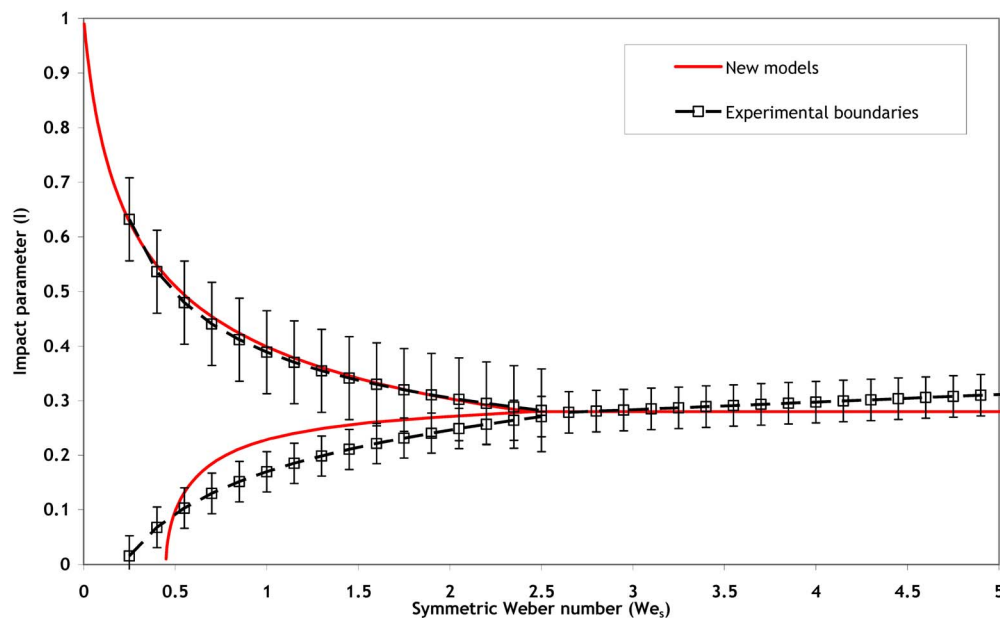
FIG. 11. (Color online) Comparison between the experimental boundaries (error bars standing for three standard deviations) and the new proposed models.

D. Discussion

Summarizing the results plotted in Fig. 6, it appears that the simple models presented above are sufficient to describe the transition curves between regimes, regardless of the diameter ratio, within the approximation of experimental uncertainty [with the exception of a We of order unity in Fig. 7(c), where the error is a little larger]. They may thus be used instead of the Ashgriz and Poo[6] expressions which, when transformed in terms of the symmetric Weber number, still rely on the diameter ratio. The new models are plotted for comparison with the experimental boundaries between regimes in Fig. 11.

In any particular case, a choice of formulas may be dictated by Figs. 7(c) and 7(d).

E. Collision outcomes at higher values of the Weber number

There is presently, to our knowledge, no experiment in the literature describing collision outcomes for a symmetric Weber number higher than 2.5 (that is for values of the classical Weber higher than 120). To complete this gap at high Weber numbers, pictures of collisions occurring with droplet velocities up to 10 m s^{-1} were obtained and analyzed using the experimental setup presented above. In spite of the large domain of symmetric Weber number under consideration (2.5–6, corresponding to 120–280 in terms of We), no coalescence outcome was observed. As shown in Fig. 11, in the range of We$_s$ > 2.5, there are only separation regimes, namely, reflexion and stretching. Furthermore, the boundary limit between the two regimes appears to be for a quasiconstant critical impact parameter I_c of around 0.28. There is neither, to our knowledge, any available model in the literature to characterize the transition between these two separation outcomes for high Weber number. A simple approach is therefore proposed here.

The basic hypothesis of this model arises from the incapacity of the surface tension forces to overpass the stretching and reflexive forces due to the high kinetic energy. That is, only kinetic energy is of importance for the determination of outcomes at high Weber number. Then, the competition between parts that contribute to reflexive or stretching separation has to be considered. To describe this competition, a dimensionless number is proposed as the ratio of the reflexive kinetic energy E_{eff} (defined in Sec. V B) and the stretching kinetic energy $E_{\text{kin } y}$ (defined in Sec. V C)

$$R_{\text{ref/stret}} = \frac{E_{\text{kin } x} - kE_{\text{kin}}}{E_{\text{kin}}I^2} = \frac{1 - I^2 - k}{I^2}. \tag{33}$$

It is expected that the transition occurs when this number is of order unity. Solving for I, the criterion is

$$I = \sqrt{\frac{1 - k}{1 + R_{\text{ref/stret}}}}. \tag{34}$$

According to the value of the viscous dissipation coefficient $k = 0.92$ (see Sec. V B and the dimensionless number $R_{\text{ref/stret}} = 0.25$, determined by our experimental results, a constant value of I is obtained for the boundary curve between reflexive and stretching separation. The low value of $R_{\text{ref/stret}}$ may be explained by the importance of viscous dissipation during the collision for low impact parameter values.

As observed in Fig. 11, the new proposed model is in good agreement with experimental measurements that characterize the transition between reflexive and stretching separation for We$_s$ > 2.5.

VI. CONCLUSION

Phenomena following droplet collisions in sprays have been investigated, in a range of parameters appropriate to systems used in a nuclear reactor containment in case of a hypothetical severe accident, that is for water droplet diameters between 220 and 450 μm and velocities between 3 and 10 m s^{-1}. This work has been carried out with an experimental setup built for this purpose at IRSN. Using a specially developed automatic postprocessing system, an extensive collection of collision pictures has been obtained and analyzed in order to determine their outcomes, for various values of the Weber number and impact parameter. Due to the large number of data and a precise assessment of measurements uncertainties (which is often missing in the literature on this topic), boundaries between domains are defined in a precise way. Results for different droplet sizes are shown to be different as the coalescence outcome domain increases for low values of the droplet diameter ratio.

For a unification of results, a new formulation of the Weber number, called here the symmetric Weber number is defined from first principles. This number involves symmetrically the energies of both droplets which are relevant in a collision. It is demonstrated that using only this number together with the impact parameter allows a unification of all our experimental results obtained for droplet collisions with different diameter ratios. In other words, the unpleasant perspective of having to consider three-dimensional representations (Weber number, impact parameter, droplet diameter ratio) is here eliminated.

Ashgriz and Poo[6] models describing the transition from coalescence to separation are in agreement with our data, within experimental uncertainty. However, it appears that Ashgriz and Poo[6] formulas when translated in terms of the new symmetric Weber number still depend on the droplets diameter ratio.

We therefore propose two new simple models to describe the boundaries between the coalescence and separation regimes in terms of the symmetric Weber number. Their formulations are associated with a physical description of the parts of kinetic and surface energy associated to each specific collision outcome. The low viscous dissipation in water is simply accounted for by a single constant coefficient. These new models provide formulas independent of the droplets diameter ratio. These formulas are much simpler than Ashgriz and Poo's[6] ones and yet capture the essential of the physics (see Fig. 11).

To explore a higher range of Weber number values, experiments of droplet collisions were also performed with higher droplet velocities. They show only two possible separation outcomes, namely, the reflexive and stretching separation. A new model is proposed to characterize the transition between these two regimes, on the basis of the relevant parts of kinetic energies defined for our other models. By construction, this new model is consistent with the above ones and is in good agreement with experiment (see Fig. 11).

It is intended to use the models proposed in this paper in a numerical calculation of the evolution of a cloud of water droplets undergoing collisions.

APPENDIX: ASHGRIZ AND POO DROPLET COLLISION MODELS

Ashgriz and Poo[6] used the We and I parameters to obtain a map of the different collision outcomes from which they fitted their model. They considered water droplets colliding at low velocities ($10 < \mathrm{We} < 100$). They showed that the previous model of Brazier-Smith *et al.*[1] did not provide a good prediction of the boundary curves between stretching separation and coalescence for a diameter ratio $\Delta = 0.5$. On the basis of their experiments, they constructed models for drops separating with the "reflexive separation" and "stretching separation" mechanisms. In this way they developed expressions for the transition curves between the various outcomes.

1. Head-on collision

For head-on or nearly head-on collisions, they proposed to define the coalescence/reflexive separation boundary in terms of an energy balance: the reflexive separation is supposed to appear when the effective kinetic energy of combined mass exceeds 75% of the final drop surface energy (this specific value was fitted according to their experimental results). Their expression for the transitional curve between coalescence and reflexive separation then is

$$\mathrm{We}_I = \left[\frac{3(7(1+\Delta^3)^{2/3} - 4(1+\Delta^2))\Delta(1+\Delta^3)^2}{(\eta_2 + \Delta^6 \eta_1)} \right], \quad \text{(A1)}$$

where $\eta_1 = 2(1-\zeta)^2(1-\zeta^2)^{1/2} - 1$, $\eta_2 = 2(\Delta-\zeta)^2(\Delta^2 - \zeta^2)^{1/2} - \Delta^3$, and $\xi = (1/2)I(1+\Delta)$.

2. Off center collision

Considering the stretching separation which occurs at a higher impact parameter, Ashgriz and Poo[6] assume that only a part of the fluid volume of each droplet interacts during collision.

This volume V_i is defined as a fraction Φ of the initial droplets volumes V

$$\Phi_s = \begin{cases} 1 - \dfrac{1}{4\Delta^3}(2\Delta - \tau)^2(\Delta + \tau) & \text{for } h > \dfrac{1}{2}d_s, \\[2ex] \dfrac{\tau^2}{4\Delta^3}(3\Delta - \tau) & \text{for } h < \dfrac{1}{2}d_s, \end{cases} \quad \text{and}$$

$$\Phi_l = \begin{cases} 1 - \dfrac{1}{4}(2 - \tau)^2(1 + \tau) & \text{for } h > \dfrac{1}{2}d_l, \\[2ex] \dfrac{\tau^2}{4}(3 - \tau) & \text{for } h < \dfrac{1}{2}d_l, \end{cases}$$

(A2)

where $\tau = (1-I)(1+\Delta)$ and $h = (1/2)(d_l + d_s)(1-I)$ represents the height of the interacting volumes.

The kinetic stretching energy of the noninteracting parts of the droplets is compared to the surface energy of a cylinder, which provides a good representation of the ligament formed during the collision. The ratio of these quantities provides an expression of the transitional Weber number between coalescence and stretching separation

$$\text{We}_{II} = \frac{4(1 + \Delta^3)^2 [3(1 + \Delta)(1 - I)(\Delta^3 \Phi_s + \Phi_l)]^{1/2}}{\Delta^2 [(1 + \Delta^3) - (1 - I^2)(\Phi_s + \Delta^3 \Phi_l)]}. \quad (A3)$$

[1] P. R. Brazier-Smith, S. G. Jennings, and J. Latham, "The interaction of falling water droplets: Coalescence," Proc. R. Soc. London, Ser. A **326**, 393 (1972).

[2] R. W. Park, "Behaviour of water drops colliding in humid nitrogen," Ph.D. thesis, University of Wisconsin, 1970.

[3] P. J. O'Rourke and F. V. Bracco, "Modelling of drop interactions in thick sprays and a comparison with experiments," *Stratified Charge Auto Engines Conference*, November 1980 (Institution of Mechanical Engineering of London, London, 1980), p. 101.

[4] J. Nijdam, B. Guo, M. Valencia-Bajarano, and T. Langrish, "An experimental investigation of agglomeration with one and two nozzle atomisation," Chin. J. Chem. Eng. **12**, 750 (2004).

[5] K. V. Beard and H. R. Pruppacher, "An experimental test of theoretically calculated collision efficiencies of cloud drops," J. Geophys. Res. **73**, 6407, doi:10.1029/JB073i020p06407 (1968).

[6] N. Ashgriz and J. Y. Poo, "Coalescence and separation in binary collisions of liquid drops," J. Fluid Mech. **221**, 183 (1990).

[7] J. P. Estrade, "Etude expérimentale et modélisation de la collision de gouttelettes," Ph.D. thesis, Ecole Nationale Supérieure de l'Aéronautique et de l'Espace, France, 1998.

[8] Y. J. Jiang, A. Unumera, and C. K. Law, "An experimental investigation on the collision behaviour of hydrocarbons droplets," J. Fluid Mech. **234**, 171 (1992).

[9] G. H. Ko and H. S. Ryou, "Modelling of droplet collision-induced breakup process," Int. J. Multiphase Flow **31**, 723 (2005).

[10] L. E. Kollar, M. Farzaneh, and A. R. Karev, "Modeling droplet collision and coalescence in an icing wind tunnel and the influence of these processes on droplet size distribution," Int. J. Multiphase Flow **31**, 69 (2005).

[11] A. Frohn and N. Roth, *Dynamics of Droplets* (Springer, New York, 2000), pp. 66–67.

[12] O. W. Jayaratne and B. J. Mason, "The coalescence and bouncing of water drops at an air/water interface," Proc. R. Soc. London, Ser. A **280**, 545 (1964).

[13] S. G. Bradley and C. D. Stow, "Collisions between liquid drops," Philos. Trans. R. Soc. London, Ser. A **287**, 635 (1978).

[14] J. Qian and C. K. Law, "Regimes of coalescence and separation in droplet collision," J. Fluid Mech. **331**, 59 (1997).

[15] J. P. Virepinte, "Etude du comportement dynamique et thermique de gouttes en régime d'interaction dans le cas de jets rectilignes," Ph.D. thesis, Ecole Nationale Supérieure de l'Aéronautique et de l'Espace, France, 1999.

[16] M. Orme, "Experiments on droplet collisions, bounce, coalescence and disruption," Prog. Energy Combust. Sci. **23**, 65 (1997).

[17] C. Gotaas, P. Havelka, H. A. Jakobsen, H. Svendsen, M. Hase, N. Rioth, and B. Weigand, "Effect of viscosity on droplet-droplet collision outcome: Experimental study and numerical comparison," Phys. Fluids **19**, 102106 (2007).